DOI: https://doi.org/10.68732/1f44fe5808ce0d87

ISBN: 978-9989-2053-6-1

Effect of Biot-Willis Coefficient in Coupled Hydro-Mechanical Hydraulic Fracturing Analysis

K. Kishida, Y. Tatemura & H. Yasuhara
Department of Urban Management, Kyoto University, Kyoto, Japan
kishida.kiyoshi.3r@kyoto-u.ac.jp
0000-0003-1588-4024, 0000-0003-4557-4692

S. Ogata
Osaka University, Suita, Japan

Abstract

Hydraulic fracturing is widely used for in-situ stress measurement and the development of enhanced geothermal systems (EGS), in which fluid is injected to create and propagate fractures. Accurate evaluation of stress state and fracture propagation requires a simulation framework that can reproduce the coupled processes of fluid flow and rock deformation.

This study develops a fully coupled hydro-mechanical simulation model for flow-rate–controlled hydraulic fracturing, implemented within a finite element method (FEM) framework, incorporating pore pressure diffusion and the resulting mechanical response within a porous rock mass. Particular attention is given to the Biot–Willis coefficient α and the initial permeability within the framework of poroelastic theory. The coefficient α governs the contribution of pore pressure to effective stress, whereas the initial permeability controls fluid diffusion and leak-off behavior.

FEM-based numerical simulations are conducted to evaluate the effects of α and permeability on injection pressure during fracture initiation and propagation, as well as on pressure behavior after injection shut-in. The results show that injection pressure decreases with increasing α due to the enhanced contribution of pore pressure to effective stress. However, this effect diminishes as α approaches approximately 0.9, beyond which the influence of α saturates.

In contrast, permeability strongly affects both breakdown pressure and post shut-in pressure decay. Lower permeability results in higher breakdown pressure due to reduced fluid leak-off, whereas higher permeability leads to rapid pressure dissipation after shut-in owing to enhanced fluid diffusion into the surrounding rock matrix.

These results indicate that the Biot–Willis coefficient primarily governs effective stress reduction and fracture initiation, while permeability controls fluid transport and pressure decay. The findings provide useful guidance for parameter identification in coupled hydro-mechanical simulations and contribute to improving the reliability of in-situ stress estimation and geothermal reservoir analysis.

Keywords

Hydraulic fracturing, Fluid–solid interaction, Biot–Willis coefficient, Poroelasticity, Injection pressure.

1 Introduction

Hydraulic fracturing is widely used for in-situ stress measurement and geothermal reservoir stimulation, in which fluid is injected into an isolated borehole interval to create fractures and estimate in-situ stress from the fluid pressure and fracture orientation (Hubbert and Willis, 1957). Accurate evaluation of this process requires a numerical framework capable of reproducing both the stress field and fracture propagation.

Previous studies (Izawa et al., 2020; Ikeda et al., 2024) have mainly employed pressure-controlled conditions, whereas actual operations are often conducted under flow-rate-controlled conditions. To better represent such conditions, this study develops a coupled hydro-mechanical model incorporating flow-rate control. In addition, since pressure behavior after injection shut-in has received limited attention, the model is designed to reproduce the entire process from fracture initiation to stress release.

Within the poroelastic framework based on Biot's theory, particular attention is given to the Biot–Willis coefficient α and the initial permeability. The coefficient α governs the contribution of pore pressure to effective stress, while permeability controls fluid diffusion and leak-off behavior. This study investigates how these parameters influence pressure response, especially after shut-in.

2 Numerical method

2.1 Outline of numerical method

In this study, numerical simulations were performed using an externally coupled framework combining COMSOL Multiphysics (finite element analysis) and MATLAB. A hydro-mechanical coupled analysis is first conducted in COMSOL, after which the damage variable and permeability are updated in MATLAB and fed back into the finite element model. This iterative procedure is repeated throughout the simulation.

2.2 Governing equations

The stress–strain behavior of the rock mass is described using the equilibrium equation and a constitutive relation incorporating pore pressure based on Biot's poroelastic theory (Biot, 1961; Ogata et al., 2020):

$$\boldsymbol{\nabla} \cdot \boldsymbol{\sigma} + \boldsymbol{F}_v = 0 \tag{1}$$

$$\boldsymbol{\sigma} = \boldsymbol{C}\colon \boldsymbol{\varepsilon} + \alpha p \boldsymbol{I}, \tag{2}$$

where σ, ε, C, and p denote the stress tensor, strain tensor, elastic stiffness tensor, and pore pressure, respectively. The Biot–Willis coefficient α represents the contribution of pore pressure to effective stress. Fluid flow is described by Darcy's law.

2.3 Damage theory, permeability and failure criteria

Fracture initiation and propagation are represented using an isotropic damage model. A scalar damage variable $D(0 \le D \le 1)$ is introduced to describe material degradation, and its effect on stiffness and permeability is expressed as:

$$E = (1 - D)E_0 \tag{3}$$

$$k = k_0 \exp(\alpha_k D) \tag{4}$$

Failure is evaluated using a tensile criterion and the Mohr–Coulomb criterion based on principal stresses. Once failure occurs, the damage variable is updated according to the corresponding strain-based evolution law. Damage is assumed to be irreversible, and an upper limit of $D = 0.99$ is imposed for numerical stability.

2.4 Consideration of rock heterogeneity

Rock heterogeneity was represented using a two-parameter Weibull distribution (Zok, 2017):

$$f(u) = \frac{m}{u_0}\left(\frac{u}{u_0}\right)^{m-1} \exp\left\{-\left(\frac{u}{u_0}\right)^{m}\right\}, \tag{5}$$

where u denotes the material property assigned to each element, u_0 is the scale parameter, and m is the shape parameter controlling the degree of variability. In this study, m=4 was adopted based on previous work (Okita et al., 2025). The distribution was applied to the spatial variability of compressive strength, tensile strength, and Young's modulus.

2.5 Analysis conditions

The analysis was conducted using a square domain with a side length of 5 m containing a circular cavity with a diameter of 0.08 m at its center, as shown in Fig. 1. The cavity diameter was selected to represent a typical borehole diameter used in hydraulic fracturing tests (approximately 76–100 mm). The domain was discretized into 28,552 triangular elements. The interior of the cavity was modeled as a fictitious porous region with extremely high porosity and permeability, and it was assumed that Biot's poroelastic theory is also valid within this region.

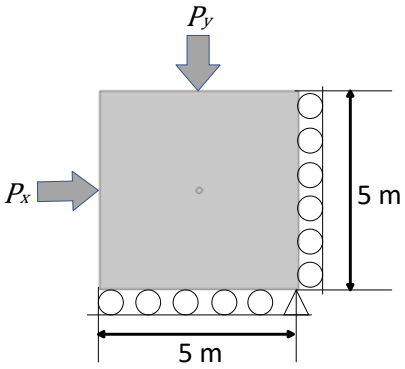


Fig. 1 Numerical model and boundary condition.

Normal stresses p_x and p_y were applied to the top and left boundaries, respectively, while roller boundary conditions were imposed on the bottom and right boundaries. Fluid flow was assumed to follow Darcy's law, and a constant flow rate was injected into the cavity. The fluid was assumed to be incompressible.

The parameters used in the analysis are listed in Table 1. The rock properties were determined assuming andesite, based on previous studies (Heap and Kennedy, 2016; Fujii et al., 2024). The in-situ stress condition corresponds to a depth of 250 m in rock with a unit weight of 25 kN/m³, resulting in an overburden pressure of 6.25 MPa. Lateral stress was applied accordingly. Hydrostatic pressure was imposed as a boundary condition within the cavity and along the outer boundary of the domain.

To consistently simulate the behavior from fracture initiation to post-injection response, fluid injection was stopped 8 s after the start of injection. Stress release was initiated at 11 s, and the analysis was terminated at 17 s. Stress release was achieved by introducing a fluid outlet at the center of the cavity, allowing fluid to be discharged and the pressure to decrease to the hydrostatic level.The analysis was performed for ten cases of the Biot–Willis coefficient and three cases of the initial permeability (Table 2).

Table 1. Parameters for the numerical simulation.

Parameter	**Value**	**Parameter**	**Value**
Young's modulus E [GPa]	20.5	Uniaxial compressive strength f_c [MPa]	25.3
Uniaxial tensile strength f_t [MPa]	3.50	Densityρ [kg/m^3]	2551
Internal friction angle θ [°]	45	Poisson's ratio [-]	0.2
Porosity n [-]	0.042	Damage-permeability coefficient α_k [-]	10
Maximum principal stress p_x [MPa]	7.5	Minimum principal stress p_y [MPa]	5
Hydrostatic pressure p_h [MPa]	2.5	Injection rate Q [mL/s]	0.,25

Table 2. Numerical simulation Cases.

Case	**Biot-Willis coefficient,α**	**Initial permeability [m^2]**	**Case**	**Biot-Willis coefficient,α**	**Initial permeability [m^2]**
Case 1	0.9	1.0×10^{-16}	Case 2	0.8	1.0×10^{-16}
Case 3	1.0		Case 4	0.9	5.0×10^{-17}
Case 5	0.9	2.0×10^{-16}	Case 6	0.6	
Case 7	0.7		Case 8	0.91	1.0×10^{-16}
Case 9	0.92	1.0×10^{-16}	Case 10	0.93	
Case 11	0.94		Case 12	0.95	

3 Results and discussions

In this study, the peak value of the pressure history under flow-rate-controlled conditions is defined as the breakdown pressure.

3.1 Influence of Biot–Willis coefficients α

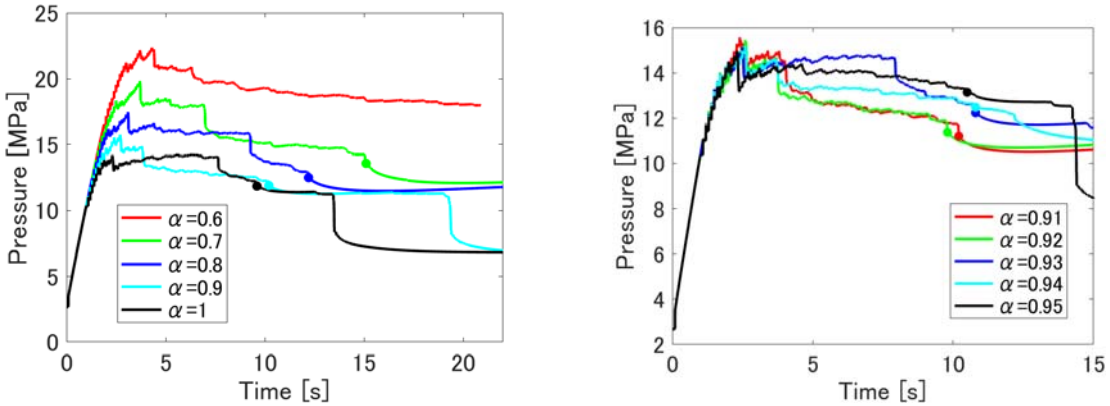
Fig. 2 shows the time histories of injection pressure for different values of the Biot–Willis coefficient α. The markers indicate the time at which the fracture reaches the outer boundary of the computational domain. Once the fracture reaches the boundary, fluid flows out of the domain, causing a rapid pressure drop. Therefore, the discussion focuses on the time period prior to these marker points. It should be noted that, for α = 0.6, the fracture does not reach the boundary even at *t*=20 s.

Fig.3 shows the fracture propagation pattern at *t*=10.2 s for α = 0.9. The fracture propagates along the maximum principal stress direction and reaches the boundary, which is consistent with the imposed stress field.

As shown in Fig. 2(a), the injection pressure decreases with increasing α. However, this decrease becomes less pronounced as α increases, and no significant difference is observed between α = 0.9 and α = 1. This behavior is explained by the effective stress relation $\sigma' = \sigma - \alpha p$, where a larger α enhances the contribution of pore pressure, leading to a greater reduction in effective stress. As α approaches unity, this effect becomes saturated.

Additional simulations for α = 0.91–0.95 (Fig. 2(b)) show no clear monotonic trend, and slight reversals in injection pressure are observed. This indicates that the influence of α saturates around α ≈ 0.9, beyond which other factors such as permeability and fracture propagation behavior become relatively dominant.

From the viewpoint of hydraulic fracturing theory, the pressure immediately before the fracture reaches the boundary can be regarded as slightly higher than the fracture closure pressure. A comparison with the minimum principal stress ($p_y = 5$ MPa) shows that this pressure approaches the theoretical value as α increases. Since the Biot–Willis coefficient varies depending on rock type and geological conditions, it should be identified through inverse analysis in practical applications.



(a) α = 0.6–1.0; (b) α = 0.91–0.95 (zoomed-in range)

Fig. 2 Time histories of injection pressure for different Biot–Willis coefficients α. Markers indicate the time when the fracture reaches the outer boundary of the computational domain.

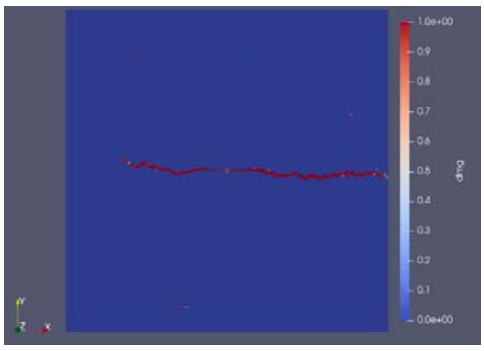


Fig. 3 Fracture propagation pattern at $t = 10.2$s for α = 0.9.The fracture propagates along the maximum principal stress direction and reaches the right boundary.

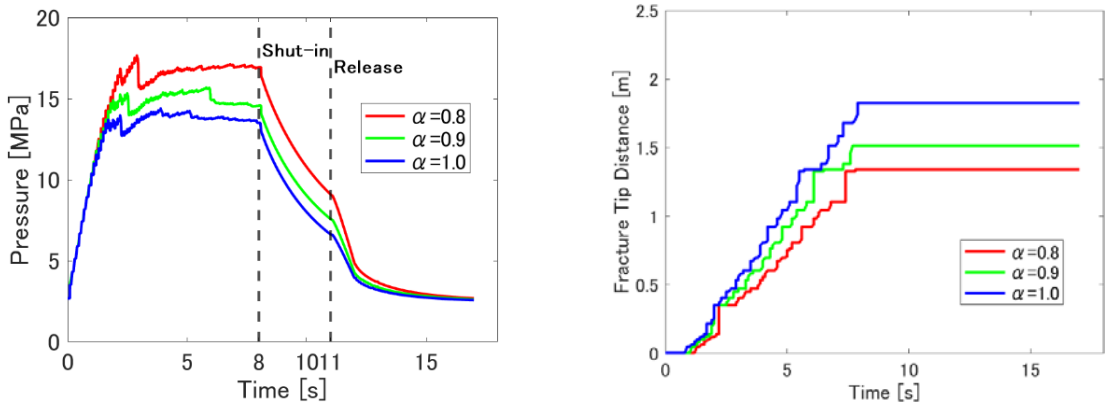
3.2 Pressure response after shut-in

Results for Cases 1–3, in which fluid injection was terminated at $t = 8$s, are shown in Fig. 4. During the pressure buildup phase up to 8 s, lower values of α result in higher injection pressures, and the corresponding breakdown pressure associated with fracture propagation also increases. This trend is consistent with the results shown in Fig. 2(a).

After shut-in, the pressure decay behavior is examined. As shown in Fig. 4(a), the rate of pressure decline is approximately the same for all cases; however, cases with smaller α maintain higher pressure levels during the decay process. This is because the breakdown pressure is higher for smaller α, while the subsequent pressure decline proceeds at a similar rate across the cases.

Fig. 4(b) shows the temporal evolution of fracture tip distance for different values of the Biot–Willis coefficient α. It is observed that fracture propagation is faster at the early stage for larger α. This behavior is attributed to the enhanced contribution of pore pressure to the effective stress, which promotes fracture propagation by reducing the effective stress near the fracture tip.

As a result, under the present simulation conditions where injection is terminated at $t = 8$s, larger values of α lead to longer fracture lengths. Despite the reduction in injection pressure with increasing α, fracture propagation is nevertheless promoted. This trend is consistent with an effective stress–controlled fracture mechanism in hydraulic fracturing.



(a) Injection pressure (b) Fracture tip distance

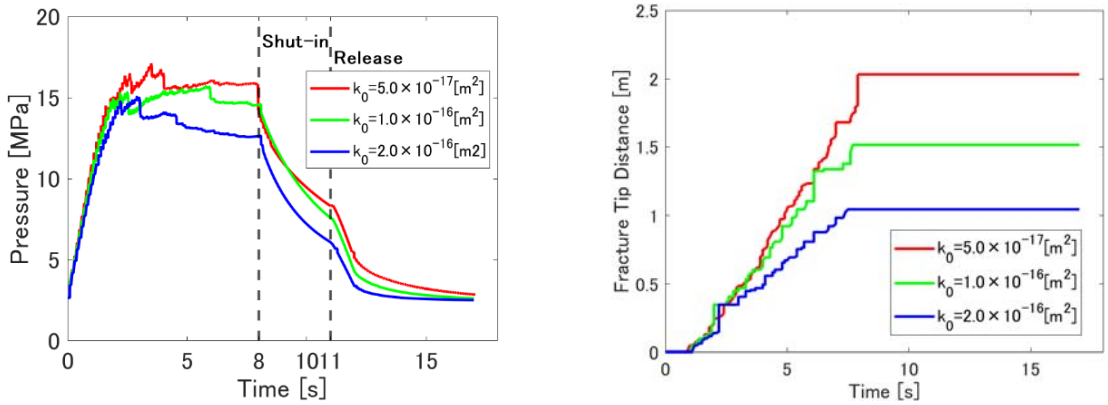
Fig. 4 Time histories of injection pressure and fracture tip distance for Cases 1–3 with injection shut-in at $t = 8$s. Dashed lines indicate the timing of shut-in and pressure release.

3.3 Effect of initial permeability on injection pressure and pressure response

Fig.5(a) shows the pressure histories for three cases with different initial permeabilities (Cases 1, 4, and 5). As observed in the figure, the breakdown pressure increases as the initial permeability decreases. This trend can be attributed to the competition between pressure accumulation within the cavity and fluid leak-off into the surrounding rock mass. In cases with higher permeability, the injected fluid rapidly infiltrates into the surrounding matrix, suppressing pressure buildup and leading to fracture initiation at lower pressures. In contrast, for lower permeability, fluid leak-off is reduced, allowing pressure to accumulate within the cavity and resulting in a higher breakdown pressure.

Focusing on the pressure behavior after shut-in at $t = 8$s, a clear difference in the rate of pressure decline is observed. Higher permeability leads to a more rapid pressure drop, as fluid diffuses more efficiently into the surrounding matrix, making it difficult to sustain the cavity pressure. These results indicate that the initial permeability strongly influences both the breakdown pressure and the pressure decay characteristics after shut-in.

Fig. 5(b) shows the temporal evolution of fracture tip distance for the same cases. Fracture propagation is more pronounced for lower permeability, resulting in longer fractures at $t = 8$s. This behavior is attributed to the suppression of fluid leak-off under low-permeability conditions, which allows fluid pressure to be maintained within the fracture. As a result, pressure is more effectively concentrated near the fracture tip, acting as a driving force for fracture propagation. This tendency is consistent with the pressure histories shown in Fig. 5(a), indicating that lower permeability leads to higher breakdown pressure and consequently promotes further fracture propagation.



(a)Time histories of injection pressure (b)Temporal evolution of fracture tip distance

Fig. 5 Effects of initial permeability on injection pressure and fracture propagation.

4 Conclusion

This study developed a fully coupled hydro-mechanical simulation model for flow-rate–controlled hydraulic fracturing and investigated the effects of the Biot–Willis coefficient α and initial permeability on pressure response and fracture behavior.

The results show that injection pressure decreases with increasing α due to enhanced effective stress reduction, while the influence of α becomes saturated around α ≈ 0.9. In contrast, initial permeability strongly affects both breakdown pressure and post shut-in pressure decay, with lower permeability leading to higher pressure buildup and longer fracture propagation due to suppressed fluid leak-off.

These findings indicate that α primarily governs fracture initiation through effective stress control, whereas permeability controls fluid transport and pressure dissipation. Furthermore, the pressure immediately before fracture boundary arrival approaches the theoretical closure pressure as α increases, suggesting that α plays a key role in the interpretation of hydraulic fracturing tests.

The proposed framework provides useful insights for parameter identification in coupled analyses and contributes to improving the reliability of in-situ stress estimation and geothermal reservoir evaluation.

References

Biot, M. A. (1961) General theory of three-dimensional consolidation, Journal of Applied Physics, Vol.12, No.2, pp.155-164.https://doi.org/10.1063/1.1712886

Fujii, T., Mori, S., Higuchi, Y., Nishida, M., Tokusu, M. and Tsutsui, S. (2024)Design and construction supervision of underground powerhouse cavern of Upper Cisokan pumped storage hydropower plant in Indonesia, Proceedings of the 50th Symposium on Rock Mechanics, JSCE.

Heap, M. J. and Kennedy, B. M.(2016) Exploring the scale-dependent permeability of fractured andesite, *Earth and Planetary Science Letters*, 447, 139-150. https://doi.org/10.1016/j.epsl.2016.05.004

Hubbert and Willis, (1957) Mechanics of Hydraulic Fracturing, *Transaction of AIME*, 210(01), 153 – 169. https://doi.org/10.2118/686-G

Ikeda, S., Ogata, S., Yasuhara, H. and Kishida, K.(2024) Numerical simulation of Hydraulic Fracturing considering Grain Boundary weakness and Fluid-Rock Heat Transfer, *ARMA*2024-0563.https://doi.org/10.56952/ARMA-2024-0563

Izawa, S., Ogata, S., Yasuhara, H., Kinoshita, N., and Kishida, K. (2020) Evaluation of Fracture Evolution of Granite during Brazilian Test by Numerical Analysis of Fracturing Process Considering Mineral Distribution, Journal of the Society of Materials Science, Japan, 69(3), 236 – 247. https://doi.org/10.2472/jsms.69.236

Ogata, S., Yasuhara, H., Kinoshita, N. and Kishida, K. (2020) Coupled thermal–hydraulic–mechanical–chemical modeling for permeability evolution of rocks through fracture generation and subsequent sealing. Computational Geosciences 24, 1845–1864. https://doi.org/10.1007/s10596-020-09948-3

Okita, R., Kishida, K., Yasuhara, H., Ogata, S.,Fujii, T. (2025) Underground cavity excavation analysis introducing damage theory and Weibull distribution, Proceedings of the 16th Japan Symposium on Rock Mechanics, Paper Number 36, pp. 193–198.

Zhu,W. and Tang, C.(2004) Micromechanical Model for Simulating the Fracture Process of Rock, *Rock Mechanics and Rock Engineering*, Vol.37, No.1, pp.25-56.https://doi.org/10.1007/s00603-003-0014-z

Zok, F. W. (2018)On weakest link theory and Weibull statistics, *Journal of the American Ceramic Society*, 100(4), 1265 – 1268.https://doi-org.kyoto-u.idm.oclc.org/10.1111/jace.14665